Extreme Mechanics Letters 1 (2014) 35–41

Contents lists available at ScienceDirect

Extreme Mechanics Letters

journal homepage: www.elsevier.com/locate/eml

Quantitative biomechanics of healthy and diseased human red blood cells using dielectrophoresis in a microfluidic system

E Du [a,1], Ming Dao [a,*], Subra Suresh [b]

[a] Department of Materials Science and Engineering, Massachusetts Institute of Technology, Cambridge, MA 02139, USA

[b] Department of Biomedical Engineering and Department of Materials Science and Engineering, Carnegie Mellon University, Pittsburgh, PA 15213, USA

HIGHLIGHTS

- A dielectrophoresis microfluidic method is established for quantitatively characterizing the mechanical properties of a large number of biological cells.
- Experiments clearly distinguish uninfected and healthy red blood cells from those infected by Plasmodium falciparum malaria parasites.
- The characterized deformability for uninfected and healthy red blood cells compare well with those derived from independent single-cell biomechanical tests that entail much greater cost, set-up time and complexity and much more limited scope and portability.

GRAPHICAL ABSTRACT

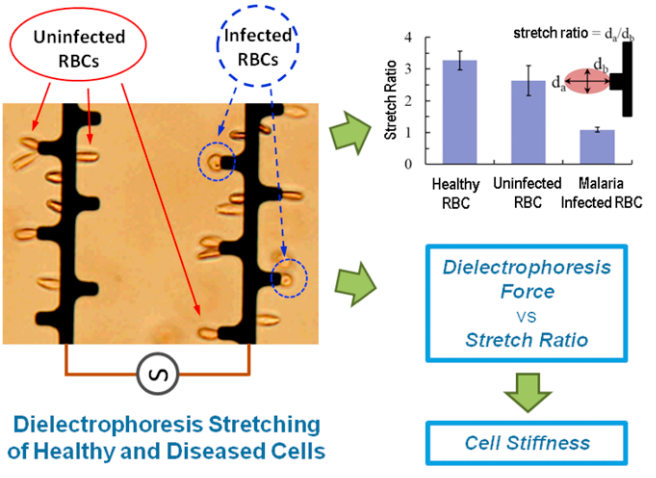

ARTICLE INFO

Article history:
Received 15 October 2014
Received in revised form 14 November 2014
Accepted 15 November 2014
Available online 9 December 2014

Keywords:
Dielectrophoresis force
Cell deformability
Malaria

ABSTRACT

We present an experimental method to quantitatively characterize the mechanical properties of a large number of biological cells by introducing controlled deformation through dielectrophoresis in a microfluidic device. We demonstrate the capability of this technique by determining the force versus deformation characteristics of healthy human red blood cells (RBCs) and RBCs infected *in vitro* with *Plasmodium falciparum* malaria parasites. These experiments clearly distinguish uninfected and healthy RBCs from infected ones, and the mechanical signatures extracted from these tests are in agreement with data from other independent methods. The method developed here thus provides a potentially helpful tool to characterize quickly and effectively the isolated biomechanical response of cells in a large population, for probing the pathological states of cells, disease diagnostics, and drug efficacy assays.

* Corresponding author.
E-mail address: mingdao@mit.edu (M. Dao).

http://dx.doi.org/10.1016/j.eml.2014.11.006
2352-4316/

[1] Present address: Department of Ocean and Mechanical Engineering, Florida Atlantic University, Boca Raton, FL, 33431, USA.

1. Introduction

Studies of the mechanics of single biological cells and cell populations offer useful insights into the mechanistic origins of human diseases, and pave the way for novel disease diagnostics, drug efficacy assays, and therapeutics [1–6]. Given the relatively simple cytoskeletal arrangement and nucleus-free structure of RBCs, the mechanics and biorheology of healthy and diseased RBCs, and their connections to blood disorders, have been topics of investigation for decades [4,7–9]. Numerous techniques are available for studying single cell biomechanics [3,5,8]. Key methods include micropipette aspiration [10,11], atomic force microscopy [12,13], optical tweezers [14–16], diffraction phase microscopy [17–19], and magnetic twisting cytometry [20]. Although these techniques have varying levels of force and displacement resolutions for probing cellular and subcellular components in living cells, they often suffer from low throughput, cumbersome experimental set-up and data interpretation, limited portability, and/or applicability only to specific testing and geometry conditions [3–5,21]. Microfluidic platforms for assessing cell biorheology, on the other hand, offer the means to probe large cell populations in high throughput [22–25], but are often limited in their flexibility to quantitatively determine specific cell mechanical properties using label-free methods (i.e., methods without using any biochemical or immunological tagging techniques).

There have been many successful efforts in utilizing dielectrophoresis (DEP) method to separate different cell populations from heterogeneous samples [26–30]. The principle of dielectrophoresis (DEP) and the ensuing electro-deformation of cells [31–33] have been employed in conjunction with microfluidic systems for biomechanical measurements of cancer cell lines [34,35] and mammalian cell lines [33,36]. But to our knowledge, DEP has not been used for quantitative, high throughput characterization of well-defined specific biomechanical properties (such as RBC membrane shear modulus) for large numbers of single cells, and to systematically invoke these biomechanics markers to distinguish between healthy and pathological states of human cells. Here we present a method that can rapidly assess the biomechanical characteristics of multiple cells simultaneously within a microfluidic chamber by recourse to DEP-induced force and electro-deformation.

In order to demonstrate the capability of this method to simultaneously test the biomechanical characteristics of many cells, we choose healthy human RBCs. We further validate this method for disease diagnostics by comparing the biomechanics of healthy RBCs with RBCs infected *in vitro* by *Plasmodium falciparum* human–malaria parasites (*Pf*-iRBCs). This choice was also motivated by the availability of results on cell mechanical properties of healthy RBCs and *Pf*-iRBCs from prior experiments conducted with other independent experimental techniques such as micropipette aspiration [37–39], optical tweezers [16,40] and microfluidics [23,24,41]. In this manner, the new results of this work could be systematically compared with other baseline work from a number of prior research studies. Although this paper focuses only on healthy RBCs and *Pf*-iRBCs, the technique presented here is conceptually applicable to study cell biomechanics in the context of other RBC-related diseases as well as to other cell-lineages.

The present work deals with a DEP method that is suitable for label-free discrimination of uninfected RBCs from *Pf*-iRBCs at its early stage, i.e. ring stage, which is the only stage found in circulating blood for diagnosis. To differentiate ring stage *Pf*-iRBCs from uninfected RBCs is critical and more challenging for the existing mechanics-based diagnostic approaches, since the modifications in mechanical properties for host cells at this stage are still relatively mild. Our method is capable of evaluating cellular mechanical properties by trapping and stretching as many as 700 RBCs per mm^2 in less than a second. We present experimental observations that reveal strong DEP trapping of healthy RBCs and uninfected RBCs, and weak DEP response of *Pf*-iRBCs over a broad range of electric frequencies.

2. Materials and method

2.1. The DEP method

DEP refers to the force exerted from the induced dipole moment on a particle by a non-uniform electric field. The DEP behavior of a particle is determined by the applied electric field, and the Clausius–Mossotti (CM) factor expressed by

$$\beta = \frac{\varepsilon_{\mathrm{p}}^* - \varepsilon_{\mathrm{m}}^*}{\varepsilon_{\mathrm{p}}^* + 2\varepsilon_{\mathrm{m}}^*}, \tag{1}$$

where the subscripts p and m stand for particle and medium, respectively, $\varepsilon^* = \varepsilon - i\sigma/\omega$ with ω being the angular field frequency, $i = \sqrt{-1}$, and ε and σ being the permittivity and conductivity, respectively, of the dielectric. The time-averaged dielectrophoresis force (DEP force) is expressed by [42]

$$\langle \boldsymbol{F}_{DEP} \rangle = 2\pi\, \varepsilon_{\mathrm{m}} r^3 \mathrm{Re}\,(\beta)\, \nabla \boldsymbol{E}_{\mathrm{rms}}^2, \tag{2}$$

where r is the radius of a spherical particle, Re( ) is the real part and $\boldsymbol{E}_{\mathrm{rms}}$ is the root mean square (rms) value of the electric field $\boldsymbol{E}$. Re(β) ranges from −0.5 to 1. When Re(β) is positive, the polarized particle moves toward the electric field maxima, under so-called positive DEP (p-DEP); when Re(β) is negative, the particle moves away from the electric field maxima, under so-called negative DEP (n-DEP). These two cases are demonstrated in Fig. 1(A).

2.2. Microfluidic device

The microfluidic device for DEP testing (Fig. 1(B) and (C)) consists of an interdigitated electrode structure and a 50 μm deep microchamber. The Ti/Au electrode of 10 nm/100 nm thickness was deposited on thin glass substrate (700 μm) using E-beam vaporization and lift-off process. The microfluidic channel was fabricated using polydimethylsiloxane (also known as PDMS) casting protocols and bonded to the glass substrate. Alternating current (AC) voltage of 3.5 V_{rms} at a frequency between 500 kHz and 50 MHz was applied to the electrode using

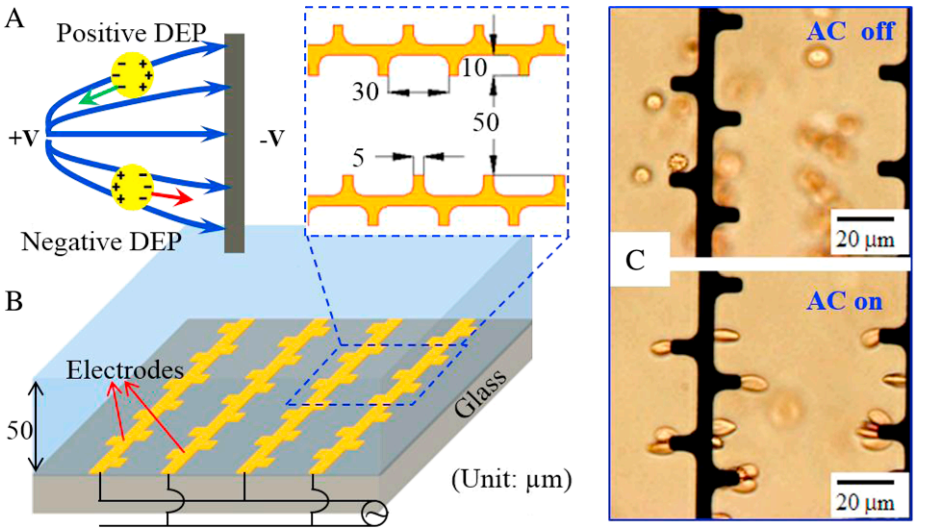

Fig. 1. DEP in a microfluidic system. A. Schematic representation of the DEP response of dielectric particles in non-uniform electric field. B. Schematic of microfluidic device with the inset (within dashed blue square) showing electrode geometries and dimensions in units of μm. C. Suspension of RBCs in static condition when the alternating current (AC) electric field is off; trapped RBCs under p-DEP when the AC electric field is on (3.5 V_{rms} and 5 MHz).

a signal generator. DEP testing of *Pf*-iRBCs and healthy RBCs was performed at room temperature and in a static condition. The cells were observed with an Olympus IX 71 inverted microscope (Olympus, Center Valley, PA, USA) using a 100 W HBO lamp. The electrode geometry was designed for maximizing single-RBC trapping at each electrode node.

2.3. Healthy and Pf-iRBCs

Healthy human RBCs free of leukocytes were procured from Research Blood Components (Brighton, MA, USA). The healthy RBCs were cultured with *P. falciparum* parasites using procedures described in detail elsewhere [43]. The cultured *P. falciparum* samples were cooled down to room temperature and synchronized at the ring stage. The samples were then washed with phosphate-buffered saline (PBS; 2.67 mmol/l KCl, 1.47 mmol/l KH_2PO_4, 137.93 mmol/l NaCl, 8.06 mmol/l $Na_2HPO_4 \cdot 7H_2O$) at 2000 rpm for 3 min at 21 °C and re-suspended in an isotonic buffer (9.25% sucrose with electrical conductivity adjusted to 0.055 S/m using PBS) for DEP analysis. The uninfected RBCs are defined as those cells that were not invaded by the *P. falciparum* parasite during cell culture. Healthy RBCs were tested in the same day of blood withdrawal using the same experimental protocol. The final concentration of RBCs was around 1% hematocrit. *Pf*-iRBCs were confirmed using a blue-fluorescent Hoechst Stain (Sigma-Aldrich, St. Louis, MO).

2.4. Image analysis and data extraction

The ImageJ software (http://imagej.nih.gov/ij/) was used to analyze the projected geometries and dimensions of RBCs. Only individually-trapped RBCs were selected for characterization. Due to the direction of the maximum DEP force for an individually-trapped RBC, it is unlikely such a trapped RBC would be significantly titled. The stretched individually-trapped RBCs were fitted with ellipses for cell shape quantification with the assumption of symmetric configuration for deformed cells in plain view. COMSOL Multiphysics (COMSOL, Inc., Burlington, MA) was used to calculate $\nabla \boldsymbol{E}^2_{rms}$ in the microfluidic DEP device. A custom script in Matlab R2009a (Matlab, Natick, MA, USA) was used to calculate the Re (β) profiles of uninfected/healthy RBCs and *Pf*-iRBCs. All data are represented as mean ± SD unless otherwise specified.

3. Results and discussion

3.1. DEP behavior of uninfected RBCs and Pf-iRBCs

Typical biological cells, such as RBCs, are composed of several components including cell membrane and cell interior. *Pf*-iRBCs are assumed to have a four-layer structure, including host cell membrane, host cell interior, parasite membrane, and parasite interior. In order to calculate the CM factor, β of RBCs surrounded by a specific medium, a smeared-out sphere method was used to approximate the effective permittivity of an N-shell sphere [44]. The N-shell sphere can be reduced to an equivalent smeared-out sphere having an effective complex permittivity

$$\begin{aligned}\varepsilon^*_{p\,\mathrm{eff}} &= \varepsilon^*_{N\,\mathrm{eff}} \\ &= \varepsilon^*_{N+1}\left[(R_{N+1}/R_N)^3 + 2\beta(\varepsilon^*_{N-1\,\mathrm{eff}}, \varepsilon^*_{N+1})\right] \Big/ \\ &\quad \left[(R_{N+1}/R_N)^3 - \beta(\varepsilon^*_{N-1\,\mathrm{eff}}, \varepsilon^*_{N+1})\right], \end{aligned} \tag{3}$$

where, from Eq. (1), $\beta\left(\varepsilon^*_{\mathrm{p}}, \varepsilon^*_{\mathrm{m}}\right) = (\varepsilon^*_{\mathrm{p}} - \varepsilon^*_{\mathrm{m}})/(\varepsilon^*_{\mathrm{p}} + 2\varepsilon^*_{\mathrm{m}})$ and ε^*_N and R_N are the complex permittivity and radius, respectively, of the shell N. We assume that the healthy and uninfected RBCs have the same dielectric constants and

Table 1
Typical values of parameters used to calculate CM factor, β, of healthy RBCs, uninfected RBCs and *Pf*-iRBCs.

Cell	Membrane thickness (nm)		Diameter (μm)	Relative permittivity, ε_r [45]		Conductivity[a], σ (S/m) [45]
Uninfected/healthy RBC	4.5		7	Membrane	4.44 ± 0.45	$<10^{-6}$
				Interior	59 ± 6	0.31 ± 0.03
Pf-iRBC	Host cell	4.5	7	Membrane	9.03 ± 0.82	$7 \pm 2 \times 10^{-5}$
				Interior	58 ± 10	$(0.95 \pm 0.05) \cdot \sigma_m$
	Parasite	5	1–3	Membrane	8 ± 4	$<10^{-6}$
				Interior	70 ± 5	1.0 ± 0.4

[a] σ_m is the electrical conductivity of the medium.

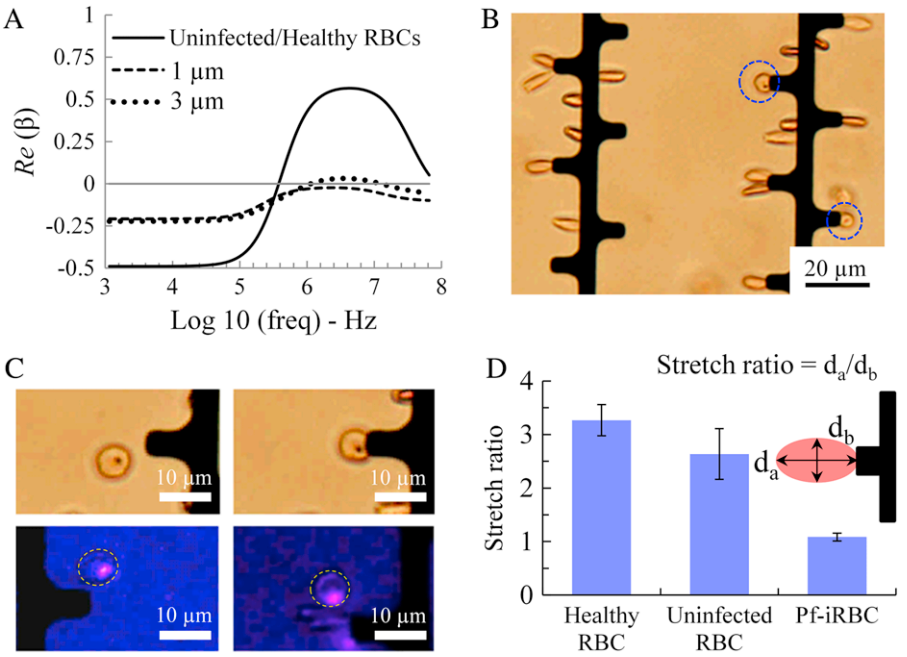

Fig. 2. Differentiation of *Pf*-iRBCs from uninfected RBCs and healthy RBCs. A. Profiles of Re(β) of uninfected/healthy RBCs and *Pf*-iRBCs using a smeared-out sphere model. B. Uninfected RBCs are trapped and stretched while *Pf*-iRBCs remain undeformed as indicated by the dashed blue circles. C. Both bright-field and fluorescence images confirm *Pf*-iRBCs undergoing a weak DEP response and essentially undeformed. D. Stretch ratio of healthy RBCs ($n = 27$), uninfected RBCs ($n = 25$) and *Pf*-iRBCs ($n = 10$) under the same electrical excitation of 3.5 V_{rms} and 3 MHz.

hence the same values of β. The effective complex permittivity of RBCs was then used to calculate Re(β) using Eq. (1) based on the parameters listed in Table 1, which were obtained from results available in the literature [45].

We observed distinctly different DEP behavior between *Pf*-iRBCs and uninfected RBCs. Fig. 2(A) shows the Re(β) profile of uninfected/healthy RBCs and *Pf*-iRBCs with parasite sizes of 1–3 μm for a first-order approximation of the early stage *Pf*-iRBCs. It can be seen that Re(β) of uninfected/healthy RBCs ranges from 0.25 to 0.6 for frequencies from 500 kHz to 5 MHz, representing a strong p-DEP effect. In contrast, for *Pf*-iRBCs, Re (β) is nearly zero for the same 500 kHz to 5 MHz frequency range, suggesting a weak DEP effect. Experimental observations confirmed this prediction (Fig. 2(B)), where uninfected RBCs and healthy RBCs were much more easily and frequently trapped at the electrode edges. This behavior also agrees with a previous report [45] that normal RBCs were trapped under a single frequency excitation at 200 kHz and traveling frequency excitation at 2 MHz while the parasitized RBCs remained free to move at both conditions.

It should be noted that beyond the p-DEP induced trapping, we observed significant stretching of healthy RBCs and uninfected RBCs as these cells are highly deformable. As shown in Fig. 2(B), the uninfected RBCs were significantly stretched while the *Pf*-iRBCs, highlighted with dashed circles, were essentially undeformed, which can be well explained by the larger stiffness and weak DEP force. Additional tests of *Pf*-iRBCs in a separate DEP test with blue-fluorescent Hoechst Stain solution (Sigma-Aldrich) (Fig. 2(C)) also confirmed this behavior. Stretching deformation was also quantified by stretch ratio, i.e., the ratio between major and minor axes of the stretched RBCs. At an applied electric excitation of 3.5 V_{rms} and 3 MHz, the stretch ratio of DEP-trapped uninfected RBCs is significantly different from those of *Pf*-iRBCs ($p < 0.001$) and healthy RBCs ($p < 0.001$) (Fig. 2(D)). This result suggests that it is possible to add shear flow in this setup to perform label-free separation of early stage *Pf*-iRBCs from uninfected RBCs and healthy RBCs as well.

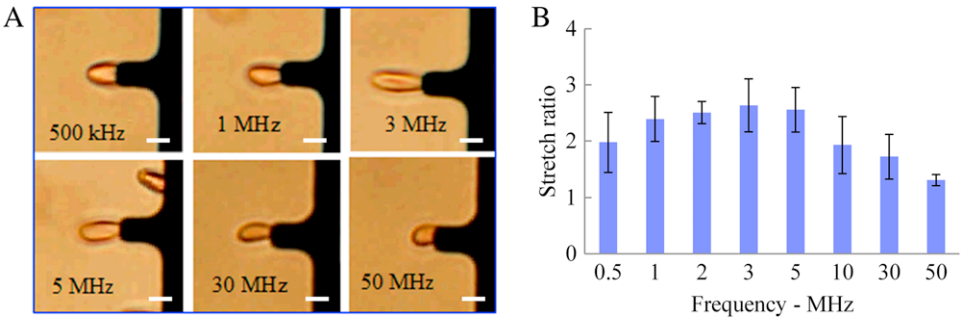

Fig. 3. Frequency-dependent cell stretching using p-DEP. A. Microscopic images of uninfected RBCs being stretched under different electric frequencies. The scale bars represent 5 μm. B. Stretch ratio of uninfected RBCs under various electric frequencies ($n = 25$).

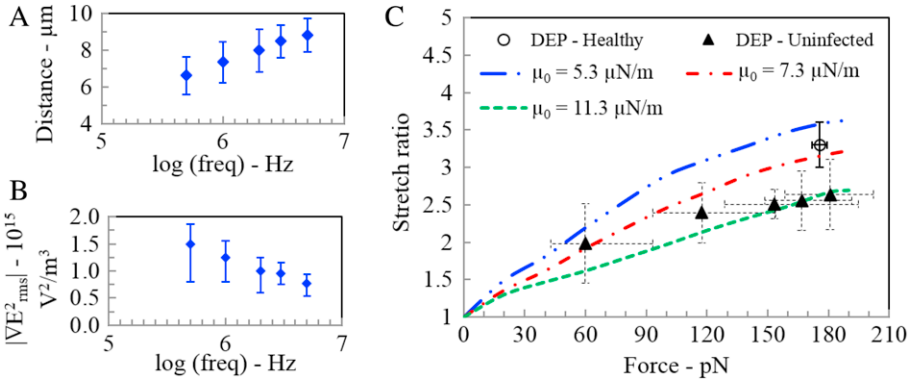

Fig. 4. Characterization of mechanical properties of healthy RBCs and uninfected RBCs using DEP stretching. A. Distance between the cell's end and the edge of electrode fingers against electric frequency for uninfected RBCs. B. The absolute value of $\nabla \boldsymbol{E}^2_{\text{rms}}$ against electric frequency for uninfected RBCs. C. Relationship of cell stretch ratio versus stretching force for healthy RBCs (circles) and uninfected RBCs (triangles) obtained from DEP approach in comparison to the experimentally-calibrated simulation results (dashed curves) for RBCs stretched by optical tweezers [16,40].

3.2. Frequency-dependent cell stretching using p-DEP

Cell-stretching using p-DEP is frequency dependent. Fig. 3(A) shows the representative microscopic images of trapping and stretching of uninfected RBCs at the edges of electrode fingers under different electric frequencies. The stretch ratio is strongly dependent on the electric frequency (Fig. 3(B)). The stretch ratio of uninfected RBCs spans from 1.3 to 2.6 with the frequency range of 500 kHz to 50 MHz. The maximum stretching is achieved when electric frequency is around 3 MHz.

3.3. Characterization of mechanical properties

Based on the measured cell deformation and the DEP force, we characterized the mechanical properties of RBCs, for frequencies of 0.5, 1, 2, 3, and 5 MHz. Uninfected RBCs showed noticeable tensile deformation. DEP force was calculated using Eq. (2). The electric field in the microfluidic device was calculated using COMSOL Multiphysics as described elsewhere [35,46]. Briefly, finite element electrostatic simulation of the electric field of a pair of electrodes within a confined microfluidic environment was conducted using the dimensions and geometries described in Fig. 2(B). The driving potentials, $\pm V_{\text{rms}}$, were applied to the electrodes while the other external boundaries were electrically insulated. The term $\nabla \boldsymbol{E}^2_{\text{rms}}$ was measured at the distance from the end of a cell to the edge of the electrode finger (equivalent to the major axes indicated in Fig. 2(D)), which was extracted from image analysis for a specific frequency (Fig. 4(A)). The absolute value of average $\nabla \boldsymbol{E}^2_{\text{rms}}$ was in the range of 7.7×10^{14}–1.5×10^{15} $\text{V}^2\ \text{m}^{-3}$ for uninfected RBCs. Relative permittivity of the medium was assumed to be 80 at room temperature, since the DEP medium was primarily composed of deionized water and a small amount of glucose and PBS [47]. Then, DEP force was estimated based on the major axes of the stretched cell for the specific frequency. Within the current frequency range, DEP force was in the range of 40–210 pN (Fig. 4(B)), with positive and negative error values calculated based on the lower and upper bounds of the values of $\nabla \boldsymbol{E}^2_{\text{rms}}$ measured for specific cell stretching conditions. The stretch ratios of healthy RBCs and uninfected RBCs against DEP force (Fig. 4(B)) were compared to the experimentally calibrated simulation results for RBCs stretched by optical tweezers [16,40]. For the healthy RBCs (shown in circles), the force versus stretch ratio relationship from DEP stretching fits well with shear modulus values between 5.3 and 7.3 μN/m; for the uninfected RBCs (shown in triangles), the force versus stretch ratio relationship from DEP stretching fits well with shear modulus values between 7.3 and 11.3 μN/m. These DEP cell deformability measurements agree well with earlier results reported in the literature [16,40], indicating that

DEP stretching is a promising method for characterization of mechanical properties of cells.

4. Conclusions

We have developed a label-free method using DEP in a microfluidic platform that is capable of providing quantitative, single-cell mechanical signatures of force as a function of electro-deformation quickly and conveniently in a portable device with the flexibility to handle over 700 cells per mm^2. The efficacy of this method has been demonstrated using interdigitated electrode arrays to distinguish early stage *Pf*-iRBCs from uninfected RBCs. The results for uninfected and healthy RBCs compare well with those derived from independent single-cell biomechanical tests that entail much greater cost, set-up time and complexity and much more limited scope and portability. The present technique offers the potential to determine the biophysical properties of large numbers of isolated cells of different types so that cell characterization with adequate statistical data can be achieved in a dynamic microfluidic platform for label-free diagnosis of a wide variety of human diseases in a cost-effective and portable device.

Acknowledgments

E.D. and M.D. acknowledge support by National Institutes of Health (R01HL094270 and U01HL114476). S.S. acknowledges support from Carnegie Mellon University. The authors thank Dr. Monica Diez-Silva for help with sample preparation.

References

[1] S. Rakshit, S. Sivasankar, Biomechanics of cell adhesion: how force regulates the lifetime of adhesive bonds at the single molecule level, Phys. Chem. Chem. Phys. 16 (6) (2014) 2211–2223.
[2] R.M. Hochmuth, Cell biomechanics: a brief overview, J. Biomech. Eng. 112 (3) (1990) 233–234.
[3] G. Bao, S. Suresh, Cell and molecular mechanics of biological materials, Nature Mater. 2 (11) (2003) 715–725.
[4] S. Suresh, Biomechanics and biophysics of cancer cells, Acta Biomater. 3 (4) (2007) 413–438.
[5] S. Suresh, J. Spatz, J.P. Mills, A. Micoulet, M. Dao, C.T. Lim, M. Beil, T. Seufferlein, Connections between single-cell biomechanics and human disease states: gastrointestinal cancer and malaria, Acta Biomater. 1 (1) (2005) 15–30.
[6] R. Schroer, H. Kiesewetter, R. Muller, Drug-improved red-cell deformability and its significance in the treatment of arterial occlusive disease, Biorheology 18 (1) (1981) 58.
[7] D. Discher, C. Dong, J.J. Fredberg, F. Guilak, D. Ingber, P. Janmey, R.D. Kamm, G.W. Schmid-Schonbein, S. Weinbaum, Biomechanics: cell research and applications for the next decade, Ann. Biomed. Eng. 37 (5) (2009) 847–859.
[8] M. Diez-Silva, M. Dao, J.Y. Han, C.T. Lim, S. Suresh, Shape and biomechanical characteristics of human red blood cells in health and disease, MRS Bull. 35 (5) (2010) 382–388.
[9] G.A. Barabino, M.O. Platt, D.K. Kaul, Sickle cell biomechanics, Annu. Rev. Biomed. Eng. 12 (2010) 345–367.
[10] S. Chien, Micropipette method for studying red and white blood-cells, Clin. Hemorheol. 5 (5) (1985) 655.
[11] M. Aingaran, R. Zhang, S.K. Law, Z.L. Peng, A. Undisz, E. Meyer, M. Diez-Silva, T.A. Burke, T. Spielmann, C.T. Lim, S. Suresh, M. Dao, M. Marti, Host cell deformability is linked to transmission in the human malaria parasite Plasmodium falciparum, Cell. Microbiol. 14 (7) (2012) 983–993.
[12] V. Lulevich, T. Zink, H.Y. Chen, F.T. Liu, G.Y. Liu, Cell mechanics using atomic force microscopy-based single-cell compression, Langmuir 22 (19) (2006) 8151–8155.
[13] P.A. Carvalho, M. Diez-Silva, H. Chen, M. Dao, S. Suresh, Cytoadherence of erythrocytes invaded by Plasmodium falciparum: quantitative contact-probing of a human malaria receptor, Acta Biomater. 9 (5) (2013) 6349–6359.
[14] R.R. Huruta, M.L. Barjas-Castro, S.T.O. Saad, F.F. Costa, A. Fontes, L.C. Barbosa, C.L. Cesar, Mechanical properties of stored red blood cells using optical tweezers, Blood 92 (8) (1998) 2975–2977.
[15] M. Dao, C.T. Lim, S. Suresh, Mechanics of the human red blood cell deformed by optical tweezers, J. Mech. Phys. Solids 51 (11–12) (2003) 2259–2280.
[16] J.P. Mills, L. Qie, M. Dao, C.T. Lim, S. Suresh, Nonlinear elastic and viscoelastic deformation of the human red blood cell with optical tweezers, Mech. Chem. Biosyst. 1 (3) (2004) 169–180.
[17] Y.K. Park, M. Diez-Silva, G. Popescu, G. Lykotrafitis, W.S. Choi, M.S. Feld, S. Suresh, Refractive index maps and membrane dynamics of human red blood cells parasitized by Plasmodium falciparum, Proc. Natl. Acad. Sci. USA 105 (37) (2008) 13730–13735.
[18] Y.K. Park, C.A. Best, T. Auth, N.S. Gov, S.A. Safran, G. Popescu, S. Suresh, M.S. Feld, Metabolic remodeling of the human red blood cell membrane, Proc. Natl. Acad. Sci. USA 107 (4) (2010) 1289–1294.
[19] H. Byun, T.R. Hillman, J.M. Higgins, M. Diez-Silva, Z.L. Peng, M. Dao, R.R. Dasari, S. Suresh, Y. Park, Optical measurement of biomechanical properties of individual erythrocytes from a sickle cell patient, Acta Biomater. 8 (11) (2012) 4130–4138.
[20] M. Puig-De-Morales-Marinkovic, K.T. Turner, J.P. Butler, J.J. Fredberg, S. Suresh, Viscoelasticity of the human red blood cell, Am. J. Physiol. Cell Physiol. 293 (2) (2007) C597–C605.
[21] M. Musielak, Red blood cell-deformability measurement: review of techniques, Clin. Hemorheol. Microcirc. 42 (1) (2009) 47–64.
[22] S.S. Shevkoplyas, T. Yoshida, S.C. Gifford, M.W. Bitensky, Direct measurement of the impact of impaired erythrocyte deformability on microvascular network perfusion in a microfluidic device, Lab Chip 6 (7) (2006) 914–920.
[23] H. Bow, I.V. Pivkin, M. Diez-Silva, S.J. Goldfless, M. Dao, J.C. Niles, S. Suresh, J. Han, A microfabricated deformability-based flow cytometer with application to malaria, Lab Chip 11 (6) (2011) 1065–1073.
[24] S. Huang, A. Undisz, M. Diez-Silva, H. Bow, M. Dao, J.Y. Han, Dynamic deformability of Plasmodium falciparum-infected erythrocytes exposed to artesunate in vitro, Integr. Biol. 5 (2) (2013) 414–422.
[25] J.S. Dudani, D.R. Gossett, H.T.K. Tse, D. Di Carlo, Pinched-flow hydrodynamic stretching of single-cells, Lab Chip 13 (18) (2013) 3728–3734.
[26] S. Fiedler, S.G. Shirley, T. Schnelle, G. Fuhr, Dielectrophoretic sorting of particles and cells in a microsystem, Anal. Chem. 70 (9) (1998) 1909–1915.
[27] J. Yang, Y. Huang, X.B. Wang, F.F. Becker, P.R.C. Gascoyne, Cell separation on microfabricated electrodes using dielectrophoretic/gravitational field flow fractionation, Anal. Chem. 71 (5) (1999) 911–918.
[28] M.P. Hughes, Strategies for dielectrophoretic separation in laboratory-on-a-chip systems, Electrophoresis 23 (16) (2002) 2569–2582.
[29] P. Gascoyne, R. Pethig, J. Satayavivad, F.F. Becker, M. Ruchirawat, Dielectrophoretic detection of changes in erythrocyte membranes following malarial infection, Biochim. Biophys. Acta, Biomembr. 1323 (2) (1997) 240–252.
[30] S.K. Srivastava, P.R. Daggolu, S.C. Burgess, A.R. Minerick, Dielectrophoretic characterization of erythrocytes: positive ABO blood types, Electrophoresis 29 (24) (2008) 5033–5046.
[31] H. Engelhardt, E. Sackmann, On the measurement of shear elastic moduli and viscosities of erythrocyte plasma membranes by transient deformation in high frequency electric fields, Biophys. J. 54 (3) (1988) 495–508.
[32] H. Engelhardt, H. Gaub, E. Sackmann, Viscoelastic properties of erythrocyte membranes in high-frequency electric fields, Nature 307 (5949) (1984) 378–380.
[33] I. Doh, W.C. Lee, Y.H. Cho, A.P. Pisano, F.A. Kuypers, Deformation measurement of individual cells in large populations using a single-cell microchamber array chip, Appl. Phys. Lett. 100 (17) (2012) 173702.
[34] I. Guido, M.S. Jaeger, C. Duschl, Dielectrophoretic stretching of cells allows for characterization of their mechanical properties, Eur. Biophys. J. Biophys. Lett. 40 (3) (2011) 281–288.
[35] J. Chen, M. Abdelgawad, L.M. Yu, N. Shakiba, W.Y. Chien, Z. Lu, W.R. Geddie, M.A.S. Jewett, Y. Sun, Electrodeformation for single cell mechanical characterization, J. Micromech. Microeng. 21 (5) (2011).
[36] L.A. MacQueen, M.D. Buschmann, M.R. Wertheimer, Mechanical properties of mammalian cells in suspension measured by electrodeformation, J. Micromech. Microeng. 20 (6) (2010) 065007.

[37] F.K. Glenister, R.L. Coppel, A.F. Cowman, N. Mohandas, B.M. Cooke, Contribution of parasite proteins to altered mechanical properties of malaria-infected red blood cells, Blood 99 (3) (2002) 1060–1063.
[38] G.B. Nash, E. O'Brien, E.C. Gordon-Smith, J.A. Dormandy, Abnormalities in the mechanical properties of red blood cells caused by Plasmodium falciparum, Blood 74 (2) (1989) 855–861.
[39] M. Paulitschke, G.B. Nash, Membrane rigidity of red blood cells parasitized by different strains of Plasmodium falciparum, J. Lab. Clin. Med. 122 (5) (1993) 581–589.
[40] M. Dao, J. Li, S. Suresh, Molecularly based analysis of deformation of spectrin network and human erythrocyte, Mater. Sci. Eng. C 26 (8) (2006) 1232–1244.
[41] M. Diez-Silva, Y. Park, S. Huang, H. Bow, O. Mercereau-Puijalon, G. Deplaine, C. Lavazec, S. Perrot, S. Bonnefoy, M.S. Feld, J. Han, M. Dao, S. Suresh, Pf155/RESA protein influences the dynamic microcirculatory behavior of ring-stage Plasmodium falciparum infected red blood cells, Sci. Rep. 2 (2012) 614.
[42] A. Ramos, H. Morgan, N.G. Green, A. Castellanos, AC electrokinetics: a review of forces in microelectrode structures, J. Phys. D: Appl. Phys. 31 (18) (1998) 2338–2353.
[43] E. Du, S. Ha, M. Diez-Silva, M. Dao, S. Suresh, A.P. Chandrakasan, Electric impedance microflow cytometry for characterization of cell disease states, Lab Chip 13 (19) (2013) 3903–3909.
[44] H. Ying, R. Holzel, R. Pethig, X.B. Wang, Differences in the AC electrodynamics of viable and nonviable yeast-cells determined through combined dielectrophoresis and electrorotation studies, Phys. Med. Biol. 37 (7) (1992) 1499–1517.
[45] P. Gascoyne, C. Mahidol, M. Ruchirawat, J. Satayavivad, P. Watcharasit, F.F. Becker, Microsample preparation by dielectrophoresis: isolation of malaria, Lab Chip 2 (2) (2002) 70–75.
[46] E. Du, S. Manoochehri, Electrohydrodynamic-mediated dielectrophoretic separation and transport based on asymmetric electrode pairs, Electrophoresis 29 (24) (2008) 5017–5025.
[47] D.P. Fernandez, Y. Mulev, A.R.H. Goodwin, J. Sengers, A database for the static dielectric constant of water and steam, J. Phys. Chem. Ref. Data 24 (1) (1995) 33–69.